Rock and Soil Mechanics

Volume 41 | Issue 4 Article 10

9-27-2020

Tunnel face stability analysis by the upper-bound finite element method with rigid translatory moving element in heterogeneous clay

Feng YANG
Key Laboratory of Engineering Structure of Heavy Railway of Ministry of Education, Central South University, Changsha, Hunan 410075, China

Shi-hua HE
School of Civil Engineering, Central South University, Changsha, Hunan 410075, China

Yao-jie WU
School of Civil Engineering, Central South University, Changsha, Hunan 410075, China

Li-yan JI
School of Civil Engineering, Central South University, Changsha, Hunan 410075, China

See next page for additional authors

Custom Citation

YANG Feng, HE Shi-hua, WU Yao-jie, JI Li-yan, LUO Jing-jing, YANG Jun-sheng, . Tunnel face stability analysis by the upper-bound finite element method with rigid translatory moving element in heterogeneous clay[J]. Rock and Soil Mechanics, 2020, 41(4): 1412-1419.

Tunnel face stability analysis by the upper-bound finite element method with rigid translatory moving element in heterogeneous clay

Authors

Feng YANG, Shi-hua HE, Yao-jie WU, Li-yan JI, Jing-jing LUO, and Jun-sheng YANG

Rock and Soil Mechanics 2020 41(4): 1412−1419 ISSN 1000−7598
https: //doi.org/10.16285/j.rsm.2019.5659 rocksoilmech.researchcommons.org/journal

Tunnel face stability analysis by the upper-bound finite element method with rigid translatory moving element in heterogeneous clay

YANG Feng[1, 2], HE Shi-hua[1], WU Yao-jie[1], JI Li-yan[1], LUO Jing-jing[1], YANG Jun-sheng[1, 2]

1. School of Civil Engineering, Central South University, Changsha, Hunan 410075, China

2. Key Laboratory of Engineering Structure of Heavy Railway of Ministry of Education, Central South University, Changsha, Hunan 410075, China

Abstract: The upper-bound finite element method with rigid translatory moving elements (UBFEM-RTME) is further improved to optimise its suitability for analysing the stability in heterogeneous clay. The method is applied to investigate the stability of the tunnel face in undrained clay layer subjected to surface surcharge. The variation of stability load σ_s/c_{u0} and the morphological characteristics and discipline of the effective discontinuities mechanism are obtained for various combinations of dimensionless buried depth ratio C/D, dimensionless gravity parameter $\gamma D/c_{u0}$ and the heterogeneous parameter $\rho D/c_{u0}$. The results reveal that C/D and $\rho D/c_{u0}$ have a significant effect on σ_s/c_{u0} and failure mechanism. $\gamma D/c_{u0}$ has a great influence on σ_s/c_{u0} but has little effect on failure mechanism. Furthermore, the UBFEM-RTME is used to show the changes of mesh failure modes under different mesh parameters such as the number and distribution of effective discontinuities, and the reasons for improving the accuracy of the upper bound solution are also explained. The applicability of UBFEM-RTME in heterogeneous clay, especially the analysis of failure mode under the limit state, is verified in comparison with the existing rigid-block upper-bound limit analysis methods and finite element bound method.

Keywords: tunnel face stability; heterogeneous clay; upper-bound finite element; critical load; failure mechanism

1 Introduction

The instantaneous stability of tunnels becomes even more important when it comes to soil strength varying with depth under undrained condition. Generally, rigid blocks upper bound method and finite element limit analysis with upper and lower bound method were applied to address this problem internationally. For circular and vertical excavation face of shallow tunnel under undrained condition, various rigid blocks failure mechanisms were proposed by Davis et al.[1]. With the consideration of heterogeneous soil, Sloan et al.[2−3] studied the stability of rectangular and circular tunnels under undrained condition using finite element limit analysis with upper and lower bound method. Augarde et al.[4] obtained upper and lower bound solution for dimensionless critical load by using this method. Wilson et al.[5] studied a series of stability problems under undrained condition by deploying rigid blocks upper bound and finite element limit analysis method. Boonchai et al.[6] discussed the stability of tunnel face whose undrained shear strength varies linearly with the depth in clay by using three dimensional finite elements.

Based on elastic-plastic finite element method with Trasca criterion, Zhou et al.[7] investigated the stability of plane strain tunnel in pure clay when cohesion changes linearly with depth. Lü et al.[8] obtained three-dimensional upper bound numerical an analytical solutions for the ultimate supporting force on the face of shielding tunnels using elastoplastic FEM. Huang et al.[9−11] deduced simplified upper bound solution for the stability supporting force in tunnel face under undrained condition in saturated clay.

From above analysis, sliding surface of tunnel under limit condition could be obtained using rigid blocks upper bound method. However, the failure mechanisms need to be predefined and are quite complex for some cases. For the heterogeneous soil in which strength varies with depth, this method may provide less accurate results. The proposed UBFEM-RTME[12−13] does not need to assume optional failure mechanisms in advance. A better bound solution and failure mechanism with slip line mesh-shaped can be obtained through changing of coordinates of elements nodes in calculation process, coupled with upgraded element nodes to increase and better distribute active discontinuities.

Up to now, only a uniform distribution of soil parameters[12−13] is considered in the UBFEM-RTME for analyzing the tunnel surface stability. In this paper, modifications were made in programs as an effort to make it applicable to evaluate the stability of tunnel in heterogeneous clay. Upper bound solution for stability of tunnel subjected to critical loading and failure mechanism of active discontinuities are expected to be obtained through further calculation amid combination of factors, which provide theoretical support for optimal tunnel construction.

Received: 14 April 2019 Revised: 5 July 2019
This work was supported by the National Natural Science Foundation of China (51878669).
First author: YANG Feng, male, born in 1981, PhD, associate Professor, mainly engaged in the research of tunnel and underground engineering. E-mail: yf5754@.csu.edu.cn
Corresponding author: YANG Jun-sheng, male, born in 1969, PhD, Professor, mainly engaged in the research of tunnel and underground engineering. E-mail: jsyang@csu.edu.cn

2 Stability analysis model of tunnel face in heterogeneous clay

2.1 Mechanical model and undrained shear strength

As shown in Fig.1, the analysis for stability of tunnel face can be described as a plain strain model along the longitudinal center-line of the tunnel. This method can help obtain changing features of collapse process[14−15]. Particularly, this assumption appears to be more suitable when the tunnel has large span.

In Fig.1, the tunnel has height D, depth C, and unit weight γ with ground surcharge σ_s. The interface between soil and rigid lining are presumed to be perfect smooth horizontally. The collapse of tunnel face is caused by ground surcharge and soil gravity.

Referring to the critical soil mechanics[16], it is known that undrained shear strength varies with depth in normally consolidated clay. In this paper, undrained shear strength in pure clay was defined as follows:

$$c_u(y) = c_{u0} + \rho(C + D/2 - y) \tag{1}$$

where $c_u(y)$ is the shear strength of the soil at depth y; c_{u0} is the undrained shear strength on the ground; ρ is the variation ratio of shear strength with depth. Under such condition, the shear strength of clay shows a heterogeneous property.

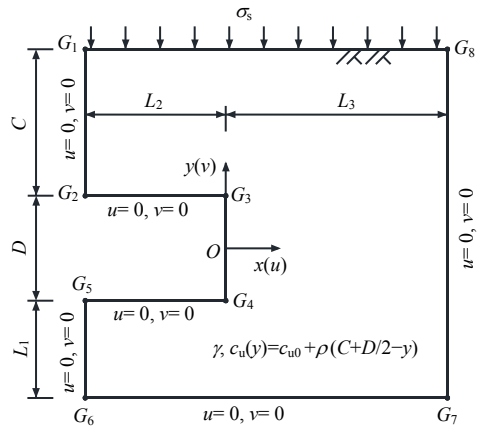

Fig.1 The stability analysis model of tunnel face in heterogeneous clay

2.2 Variables analysis and parameter selection

Stability of plain strain tunnel involves following parameters $\{\sigma_s$、C、D、c_{u0}、γ、$\rho\}$. For the convenience, parameters are transformed into dimensionless form shown as

$$\left\{\frac{\sigma_s}{c_{u0}}, \frac{\gamma D}{c_{u0}}, \frac{C}{D}, \frac{\rho D}{c_{u0}}\right\} \tag{2}$$

where σ_s/c_{u0} is the dimensionless critical load; C/D is the depth ratio; $\gamma D/c_{u0}$ is the dimensionless soil weight parameters; and $\rho D/c_{u0}$ is dimensionless parameters of strength in heterogeneous clay.

According to dimensionless stability coefficient proposed by Augarde et al[4], σ_s/c_{u0} is described as dimensionless critical load parameter to evaluate the tunnel face stability with consideration of ground surcharge load. Stability indicator $(\sigma_s - \sigma_t)/c_{u0}$ can be converted with σ_s/c_{u0}, when σ_t is set to zero along the ground surface.

Parameters are listed in Table 1 in order to study the tunnel stability for different parameters.

Table 1 Parameters of tunnel and clay

C/D	$\rho D/c_{u0}$	$\gamma D/c_{u0}$
1, 2, 3, 4, 5, 6, 7, 8, 9, 10	0, 0.25, 0.5, 0.75, 1.0, 1.25, 1.5	0, 1 ,2, 3

3 Upper bound finite element model of tunnel face in heterogeneous clay

Analysis of finite element upper bound model for tunnel face stability in heterogeneous clay is shown in Fig.1, and the initial meshes for the stability calculation are not included. The horizontal and vertical ranges of the model are respective taken as L_2+L_3 and C+D+L_1, where L_1, L_2 and L_3 are parameters related to the tunnel depth C. The selection of these values should be large enough to eliminate the boundary effects.

Tunnel face is free without traction, and the ground surface is imposed by $\int_s \bar{v}\mathrm{d}S = -1$. Other boundaries of the mode are constrained in both x and y directions, namely u=0，v=0. And origin is set at the center of tunnel face. The positive directions of x and y are towards right and up, velocity of positive direction is consistent with this.

Virtual power of soil dead-weight for the whole model P_γ is set as:

$$P_\gamma = \sum_{i=1}^{n_e} \gamma A_i v_i;\ -A_i < 0\ (i = 1, \ldots, n_e) \tag{3}$$

where n_e is the total number of elements in the domain; A_i is the area of the ith element，which is always positive.

For rigid translatory moving elements, internal dissipation energy only occurs in the velocity discontinuities, aggregate dissipation energy P_c is given by the form:

$$P_c = c_u(y) \sum_{i=1}^{n_d} \xi_i' \tag{4}$$

where $c_u(y)$ can calculated using Eq.(1); value of y is the vertical coordinate in the midpoint of discontinuities as shown in Fig.2; n_d is the total number of velocity discontinuities; and ξ_i' is an auxiliary variable for ith discontinuities. It is set as

$$\begin{aligned}\xi_i' = 1/\tan\varphi\big[&u_{r,i}(y_{f,i} - y_{s,i}) + v_{r,i}(x_{s,i} - x_{f,i}) + \\ &u_{l,i}(y_{s,i} - y_{f,i}) + v_{l,i}(x_{f,i} - x_{s,i})\big]\end{aligned} \tag{5}$$

where $u_{r,i}$ and $v_{r,i}$ are the velocity components on the clockwise side of elements in the ith velocity discontinuities; $u_{l,i}$ and $v_{l,i}$ are the velocity components on opposite side of elements in the ith velocity discontinuities; $x_{s,i}$ and $y_{s,i}$ are the starting coordinates in the ith velocity discontinuities tangentially; and $x_{f,i}$ and $y_{f,i}$ are the ending coordinates, related variables are shown in Fig.2.

https://rocksoilmech.researchcommons.org/journal/vol41/iss4/10
DOI: 10.16285/j.rsm.2019.5659

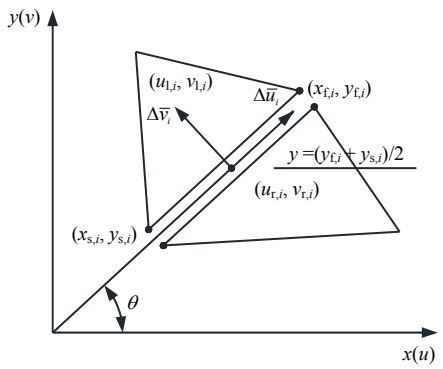

Fig.2 The discontinuity of UBFEM- RTME

For undrained shear strength parameters in heterogeneous clay, φ is fixed to zero in Eq(5). The term 1/tanφ in Eq.(5) is retained in order to reduce the numbers of unknown variables and simplify computation. A small value such as φ=0.001° is chosen when calculating. After checking, this simplification will not affect upper bound solution obtained. The results still satisfy the upper bound theorem, and the accuracy of the results can be fully guaranteed.

Another axillary variable ξ_i'' of the ith velocity discontinuity is expressed as follows:

$$\xi_i'' = u_{r,i}(x_{s,i} - x_{f,i}) + v_{r,i}(y_{s,i} - y_{f,i}) + u_{1,i}(x_{f,i} - x_{s,i}) + v_{1,i}(y_{f,i} - y_{s,i}) \tag{6}$$

As shown in Fig.2, the velocity discontinuities are imposed by associated flow rules, the constraints are written as

$$-\xi_i'' - \xi_i' \leqslant 0,\ \xi_i'' - \xi_i' \leqslant 0\ (i = 1,...,n_{\mathrm{d}}) \tag{7}$$

In order to find solution for dimensionless critical load parameter $\sigma_{\mathrm{s}}/c_{\mathrm{u0}}$ for tunnel face stability, an objective function for finite element upper bound with linear programming is developed as following:

$$\sigma_{\mathrm{s}}/c_{\mathrm{u0}} = \left(c_{\mathrm{u}}(y) \sum_{i=1}^{n_{\mathrm{d}}} \xi_i' - \sum_{i=1}^{n_{\mathrm{e}}} \gamma A_i v_i \right) \Big/ c_{\mathrm{u0}} \tag{8}$$

In addition to constraints on the velocity boundary, boundaries of the domain need to impose geometric constraints that make nodes move on the related boundaries. These boundary condition are expressed as following:

$$\left.\begin{array}{l}
G_1G_2 : x_j = -L_2,\ D/2 \leqslant y_j \leqslant D/2 + C;\ (j = 1,...,n_{\mathrm{g1}}) \\
G_2G_3 : -L_2 \leqslant x_j \leqslant 0,\ y_j = D/2;\ (j = 1,...,n_{\mathrm{g2}}) \\
G_3G_4 : x_j = 0,\ -D/2 \leqslant y_j \leqslant D/2;\ (j = 1,...,n_{\mathrm{g3}}) \\
G_4G_5 : -L_2 \leqslant x_j \leqslant 0,\ y_j = -D/2;\ (j = 1,...,n_{\mathrm{g4}}) \\
G_5G_6 : x_j = -L_2,\ -L_1 - D/2 \leqslant y_j \leqslant -D/2;\ (j = 1,...,n_{\mathrm{g5}}) \\
G_6G_7 : -L_2 \leqslant x_j \leqslant L_3,\ y_j = -L_1 - D/2;\ (j = 1,...,n_{\mathrm{g6}}) \\
G_7G_8 : x_j = L_3,\ -L_1 - D/2 \leqslant y_j \leqslant C + D/2;\ (j = 1,...,n_{\mathrm{g7}}) \\
G_8G_1 : -L_2 \leqslant x_j \leqslant L_3,\ y_j = C + D/2;\ (j = 1,...,n_{\mathrm{g8}})
\end{array}\right\} \tag{9}$$

The above model for tunnel face stability with upper bound finite element in heterogeneous soil is constructed based on existing UBFEM-RTME and its programming[17] by revising soil cohesion c and internal friction angle φ. In this connection, expression of constraints including objective function $\sigma_{\mathrm{s}}/c_{\mathrm{u0}}$, flow rules have also changed. The upper bound finite element nonlinear programming can also be solved by FMINCON and other tools. A series of mesh updating technique[12] are employed to obtain more optimal solution. Measures contain: (i) merging and deleting invalid elements; (ii) refining active mesh; (iii) mesh inheritance and revision after changing parameters. These methods can help reduce the scope of domain and make the solutions more accurate.

4 Discussion of upper bound solutions of critical loads

4.1 The analysis of upper bound solution

Using the improved UBFEM-RTME program, a series of upper bound analyses are performed on different combinations of the dimensionless parameters listed in Table 1. Table 2 shows the upper bound solutions of critical load $\sigma_{\mathrm{s}}/c_{\mathrm{u0}}$ of the tunnel face under the influence of different considered parameters. It can be concluded from the table that $\sigma_{\mathrm{s}}/c_{\mathrm{u0}}$ increases with increase of $\rho D/c_{\mathrm{u0}}$ and C/D. $\sigma_{\mathrm{s}}/c_{\mathrm{u0}}$ becomes small when $\gamma D/c_{\mathrm{u0}}$ increases. It is noted that bearing capacity of formation increases as soil strength heterogeneous parameters and depth increase. But bearing capacity decreases with increasing soil unit weight. These conclusions are consistent with those in literatures [4] and [9].

4.2 Comparison of upper bound solutions

Curves in Figs.3−5 indicate relationship between considered parameters on upper bound solutions and $\sigma_{\mathrm{s}}/c_{\mathrm{u0}}$. And the obtained results are compared with those in existing literature.

Figure 3(a) presents a comparison of upper bound solution of $\sigma_{\mathrm{s}}/c_{\mathrm{u0}}$ obtained by UBFEM-RTME with previous upper and lower bound solution[1,4,9] in homogeneous soil. The comparative data are respectively obtained from different approaches, such as, rigid blocks upper bound solution proposed by Davis et al[1], multi-block upper bound solution provided by Huang et al[9], plastic limit analysis finite element upper and lower bound solutions introduced by Augarde et al[4] by linear interpolation. It is seen that the present results are smaller than those obtained by Davis et al[1] and Huang et al[9] for the same parameters, and are between the plastic limit analysis finite element upper solution and lower bound solution introduced by Augarde[4]. When C/D=3 and $\gamma D/c_{\mathrm{u0}}$=2，the results in this paper are 16.24% and 6.9% smaller than those contributed by Davis et al[1] and Huang et al[9], respectively. Compared with results from Augarde et al[4], the average error is only 1.7%. Under upper bound theorem framework, present results appear to be more accurate.

In Fig.3(b), for cases where $\rho D/c_{\mathrm{u0}}$=1, the upper bound solution of $\sigma_{\mathrm{s}}/c_{\mathrm{u0}}$ varies with depth C/D in heterogeneous soil. It is shown that the upper limit of $\sigma_{\mathrm{s}}/c_{\mathrm{u0}}$ increases with increasing C/D; and the increase rate becomes slower when $\gamma D/c_{\mathrm{u0}}$ increases. In addition, when the buried depth increases,

the difference between the upper and lower solutions of Augarde et al. [4] slightly increases. Compared with multi-block upper-bound solutions, the upper-bound solutions of the UBFEM-RTME are always between the upper and lower solutions of Augarde et al. [4], which indicates an advanced accuracy of this method even with a larger value of buried depth. For the case of $\gamma D/c_{u0}$=2 and C/D=1, present results is 7% lower than upper bound results given by Huang et al [9], and the average error is 2.3% with comparison of upper and lower bound results presented Augarde et al [4]. When C/D increases to 3, present results are 7.5% lower than upper bound results presented by Huang et al[9], and 0.2% in average error compared with upper and lower bound solution of Augarde et al [4].

Curves of dimensionless critical load σ_s/c_{u0} varying with strength heterogeneous parameters $\rho D/c_{u0}$ are shown in Fig.4. $\gamma D/c_{u0}$=0 and $\gamma D/c_{u0}$=3 are chosen as soil weight parameters.When $\gamma D/c_{u0}$ and C/D are fixed, dimensionless critical load σ_s/c_{u0} show a linear increase with strength heterogeneous parameter $\rho D/c_{u0}$, and the gradient of curves increases with buried depth. It is noted that present results are proven to be more accurate in Fig.4.

Figure 5 shows the variation in upper-bound solutions σ_s/c_{u0} with the soil unit weight parameter $\gamma D/c_{u0}$, and C/D=1 and C/D=3 are chosen for simplified analysis. When C/D and $\rho D/c_{u0}$ are constant, the value of σ_s/c_{u0} linearly decreases with $\gamma D/c_{u0}$, and the decrease rate increases with an increase in the buried depth. Other comparison data shown in the figure prove that it is consistent with obtained conclusions.

Table 2 Results of the dimensionless critical load σ_s/c_{u0} of tunnel face

$\rho D/c_{u0}$	C/D	σ_3/c_{u0} for different $\gamma D/c_{u0}$				C/D	σ_3/c_{u0} for different $\gamma D/c_{u0}$			
		0	1	2	3		0	1	2	3
0.00		4.30	2.80	1.30	−0.20		7.60	1.10	−5.40	−11.90
0.25		5.50	4.00	2.50	1.00		17.41	10.91	4.41	2.09
0.50		6.68	5.18	3.68	2.18		27.07	20.57	14.07	7.57
0.75	1	7.84	6.34	4.84	3.34	6	36.70	30.20	23.70	17.20
1.00		8.99	7.49	5.99	4.49		46.31	39.81	33.31	26.81
1.25		10.14	8.64	7.14	5.64		55.91	49.41	42.91	36.41
1.50		11.28	9.78	8.28	6.78		65.51	59.01	52.51	46.01
0.00		5.46	2.96	0.46	−2.04		7.92	0.41	−7.09	−14.59
0.25		8.04	5.54	3.04	0.54		19.80	12.30	4.80	2.70
0.50		10.56	8.06	5.56	3.06		31.50	24.00	16.50	9.00
0.75	2	13.05	10.55	8.05	5.55	7	43.17	35.67	28.17	20.67
1.00		15.53	13.03	10.53	8.03		54.83	47.33	39.83	32.33
1.25		18.01	15.51	13.00	10.50		66.49	58.99	51.49	43.99
1.50		20.48	17.98	15.48	12.97		78.14	70.64	63.14	55.64
0.00		6.22	2.72	−0.78	−4.28		8.19	−0.31	−8.81	−17.31
0.25		10.41	6.91	3.41	0.09		22.21	13.71	5.21	−3.29
0.50		14.50	11.00	7.50	4.00		36.04	27.54	19.04	10.54
0.75	3	18.57	15.07	11.57	8.07	8	49.83	41.33	32.83	24.33
1.00		22.62	19.12	15.62	12.12		63.61	55.11	46.61	38.11
1.25		26.67	23.17	19.67	16.17		77.39	68.89	60.39	51.89
1.50		30.71	27.21	23.71	20.21		91.16	82.66	74.16	65.66
0.00		6.78	2.28	−2.22	−6.72		8.44	−1.06	−10.56	−20.06
0.25		12.73	8.23	3.73	−0.77		24.66	15.16	5.66	−3.84
0.50		18.57	14.07	9.57	5.07		40.67	31.17	21.67	12.17
0.75	4	24.37	19.87	15.37	10.87	9	56.65	47.15	37.65	28.15
1.00		30.16	25.66	21.16	16.66		72.62	63.12	53.62	44.12
1.25		35.94	31.44	26.94	22.44		88.59	79.09	69.59	60.09
1.50		41.71	37.21	32.71	28.21		104.55	95.05	85.55	76.05
0.00		7.23	1.73	−3.77	−9.27		8.66	−1.84	−12.34	−22.84
0.25		15.07	9.57	4.07	−1.43		27.14	16.64	6.13	−4.37
0.50		22.76	17.26	11.76	6.26		45.40	34.90	24.40	13.90
0.75	5	30.43	24.93	19.43	13.92	10	63.63	53.12	42.62	32.12
1.00		38.07	32.57	27.07	21.57		81.84	71.34	60.84	50.34
1.25		45.72	40.22	34.72	29.22		100.05	89.55	79.05	68.55
1.50		53.35	47.85	42.35	36.85		118.26	107.76	97.26	86.76

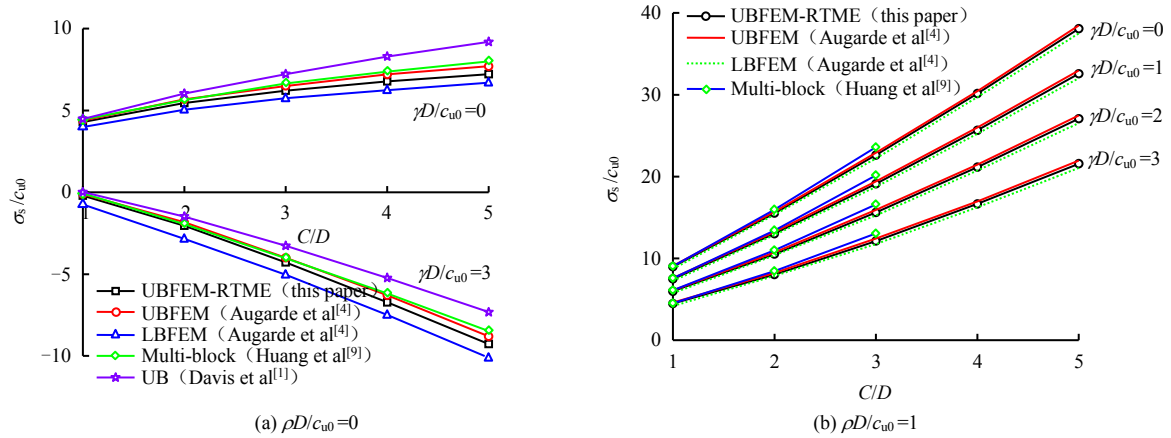

(a) $\rho D/c_{u0}$=0 (b) $\rho D/c_{u0}$=1

Fig.3 Curves of dimensionless critical load σ_s/c_{u0} for varying dimensionless buried depth ratio C/D

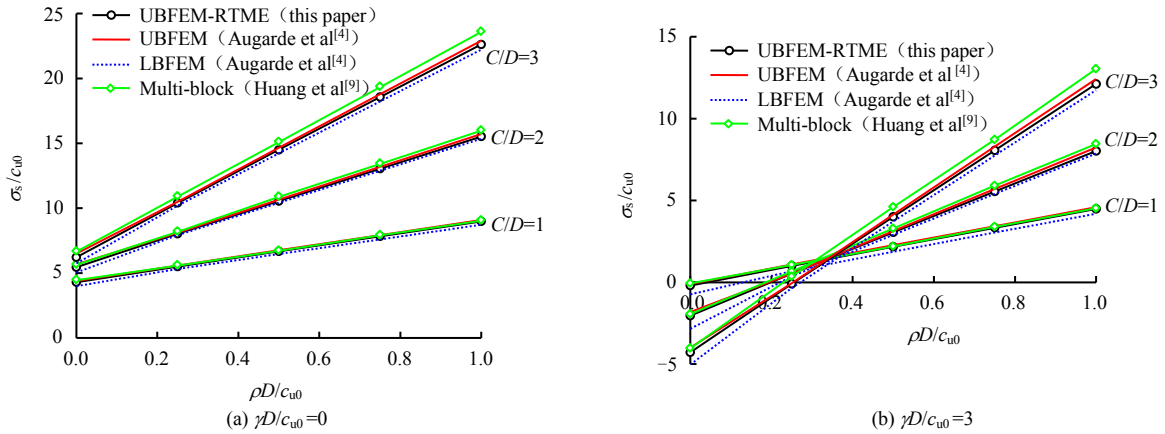

(a) $\gamma D/c_{u0}$=0 (b) $\gamma D/c_{u0}$=3

Fig.4 Curves of dimensionless critical load σ_s/c_{u0} for varying heterogeneous parameter $\rho D/c_{u0}$

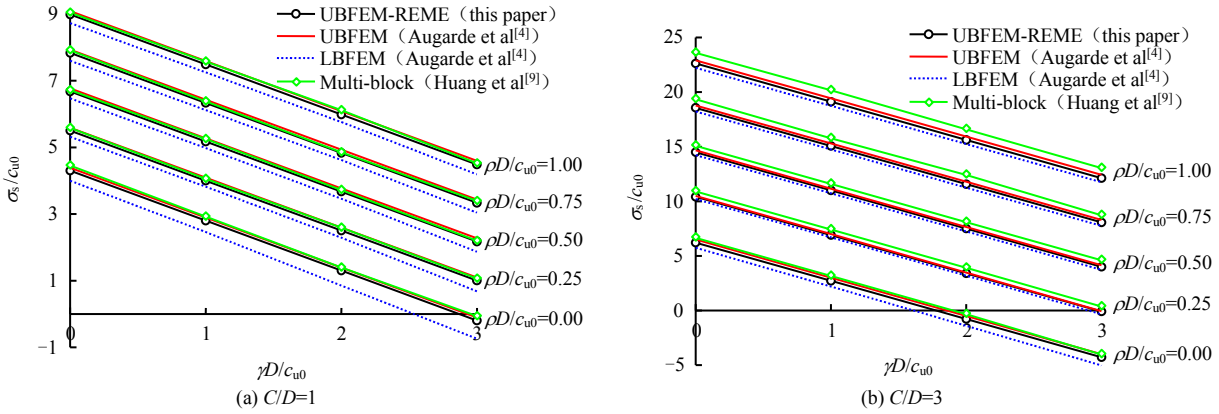

(a) C/D=1 (b) C/D=3

Fig.5 Curves of dimensionless critical load σ_s/c_{u0} for varying dimensionless gravity parameter $\gamma D/c_{u0}$

5 Discussion of failure mechanisms

5.1 Basic features of failure mechanisms for tunnel face

In addition to the upper bound solution for dimensionless critical load σ_s/c_{u0}, critical collapse mechanisms characterized by active discontinuity mesh (approximate as slip line network) in heterogeneous soil are determined by UBFEM-RTME. To determine the characteristics of failure mechanisms from different prospects, failure mode analysis of tunnel faces is shown in Fig.6 under different conditions for cases of C/D=3, $\rho D/c_{u0}$=0.5, and $\gamma D/c_{u0}$=2.

Figure 6(a) is a cloud chart of element velocity vector after normalization. It can be seen that the element velocity is higher in front of the tunnel face, while it is smaller at the ground surface. The white lines in this figure are the active velocity discontinuities, which can be used to quantitatively determine both the shape and scope of the associated plastic failure area.

Figure 6(b) presents the deformation diagram of active discontinuity mesh, which is constructed by containing velocities on both sides of elements for the active velocity discontinuity. The diagram directly reflects the failure shape of tunnel face at the critical state. It can be found that, in addition to some main sliding surfaces formed bounded by the edge of undamaged area, there are a large number of mesh-like sliding

surfaces diagonally above the tunnel face within the damaged area.

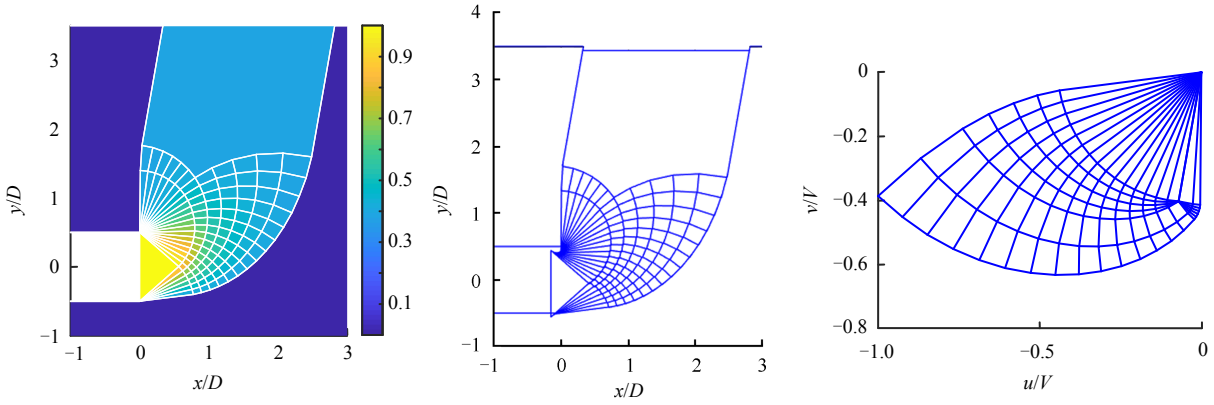

(a) Normalized element velocity contour (b) Deformation diagram with active discontinuities (c) Element velocity vector

Fig.6 The characteristic failure mode analysis of tunnel faces（C/D=3, $\rho D/c_{u0}$=0.5, $\gamma D/c_{u0}$=2, σ_s/c_{u0}=7.50）

The maximum velocity vector is set as unit value, and other velocity vectors are changing as the same rate for normalization. Then, a model velocity vector diagram is formed shown in Fig. 6(c), in which every line represents the related velocity of elements on both sides of corresponding velocity discontinuity line, which corresponds to the active discontinuity in Fig.6(a). The lines between the origin (0, 0) and any intersection represents the related velocity vector of a corresponding element in Fig. 6(a). For example, the line between the origin and the leftmost intersection point is the velocity of whole rigid block of tunnel face. The horizontal component of selected velocity has a large value of the whole model.

It is noted that rigid block upper bound method in literatures [7−9] needs to assume failure mode to determine the relationship between geometric parameters of block and the velocity field. By using proposed UBFEM-RTME method in the paper, the upper limit solution and failure mode are obtained without assumption of failure mode. Using nonlinear programming search and grid updating, the obtained results appear to be more accurate than those calculated using rigid block upper limit method. Compared with velocity vector chart introduced by Augarde et al.[4], collapse mode similar to sliding line network in this paper is more clear-cut and more distinct in range.

At present, based on limit analysis, the optimal simplified critical load and upper solution of the supporting pressure are mainly obtained by continuously optimizing the failure mechanism[7]. Compared with limit analysis of plastic element, the failure mode obtained by UBFEM-RTME method is more clear, which provide reference for simplified method. This method is expected to applied to the stability of three-dimensional tunnel face with broad prospect.

5.2 Effect of mesh density

The UBFEM-RTME method needs to update meshes during the calculation process, and the effect of updated mesh density on calculated results can't be ignored. In this connection, the effects of mesh density on dimensionless critical load σ_s/c_{u0} and collapse mode are particularly discussed. The analysis is carried out for the case of C/D=4, $\rho D/c_{u0}$=1, $\gamma D/c_{u0}$=2, the cloud diagram with velocity vector value and velocity vector diagram for different mesh densities are shown in Fig.7.

The velocity vector cloud maps corresponding to sparse mesh, slightly dense mesh and dense mesh are shown in Figs.7(a)−7(c) with total number of active discontinuities 81, 165, and 525, respectively. Figures 7(d)−7(f) are the corresponding velocity vector diagrams.

It can be seen from Figs.7(a) and 7(d) that the failure mode (slip line network) and velocity vector field obtained by sparse grid are actually consistent with those by multi-block upper bound method (or rigid block upper limit) in existing literature [9]. Only one layer of triangular block can be found in failure domain, the dimensionless critical load σ_s/c_{u0} is 22.65.

In Figs.7(b) and 7(e), as a layer of block emerges in front of tunnel face, the failure mode and velocity vector field become complex. Its corresponding dimensionless critical load σ_s/c_{u0} is 21.42, and its accuracy is improved by about 5.74%. At the same time, the collapsed area in front and behind tunnel face increases.

In Figs.7(c) and 7(f), as mesh get denser and total number of active discontinuities is 525, slip line network becomes smoother, and velocity vector field transforms into smooth mesh shape. Then, dimensionless critical load 21.16 was obtained with accuracy increased by about 1.23% compared with those calculated from slightly dense mesh Fig.7(b).

Furthermore, appropriate increase of active discontinuity can obtain more accurate mesh-shaped failure mechanism. The mesh sliding surface and velocity vector field show that collapse is more likely to occur, upper bound solution of σ_s/c_{u0} is more accurate.

5.3 Variation in failure mechanisms

The following analyses discuss the evolution of the failure mechanism of the tunnel face. Considering the shapes of active discontinuities under different situations are quite similar, the variations in the pattern of the failure mechanisms are shown in Figs.8−10. The left side of figure is the change of outer surfaces of the failure zone, while the right side is the distribution characteristic of active discontinuities within the failure zone.

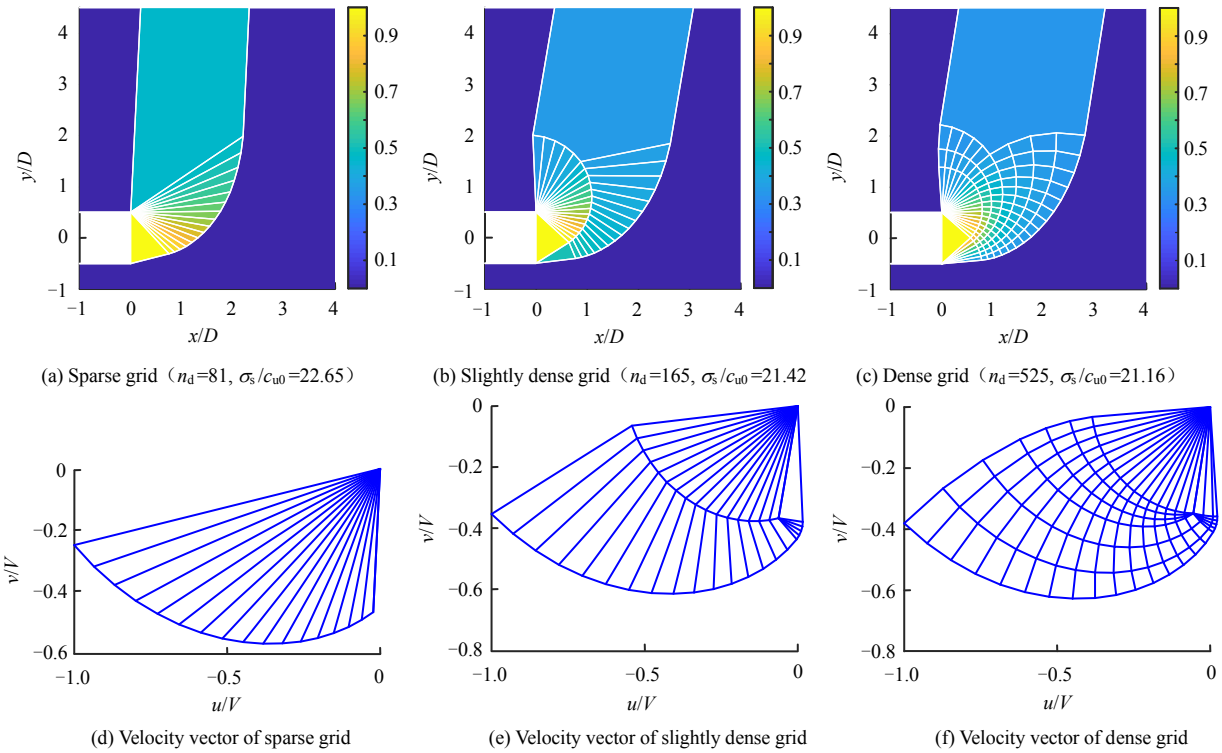

(a) Sparse grid（n_d=81, σ_s/c_{u0}=22.65） (b) Slightly dense grid（n_d=165, σ_s/c_{u0}=21.42 (c) Dense grid（n_d=525, σ_s/c_{u0}=21.16）

(d) Velocity vector of sparse grid (e) Velocity vector of slightly dense grid (f) Velocity vector of dense grid

Fig.7 Failure modes of tunnel face for different mesh densities（C/D=4, $\rho D/c_{u0}$=1, $\gamma D/c_{u0}$=2）

5.3.1 Effect of soil strength heterogeneous parameter $\rho D/c_{u0}$ on failure mechanism

Figure 8 indicates that the failure mode of tunnel face under different values of $\rho D/c_{u0}$ when depth and soil gravity parameters are fixed (C/D=4, $\gamma D/c_{u0}$=2). In case of increasing $\rho D/c_{u0}$, the failure domain shrinks, location of collapse becomes shallow, and the scope of failure domain in the surface ground diminishes. This may be caused by the increase of ρ, the shear strength difference between the upper and lower soil layers becomes larger, and the failure domain climbs up.

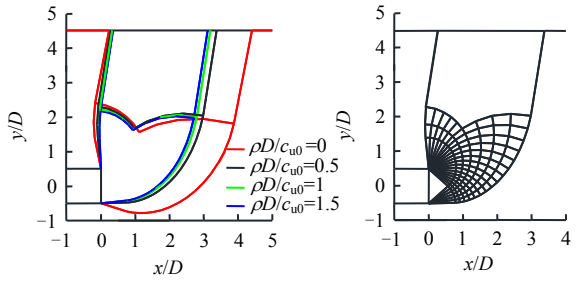

(a) $\rho D/c_{u0}$=0, 0.5, 1, 1.5 (b) $\rho D/c_{u0}$=0.5

Fig.8 Failure mechanisms of slip line network in tunnel face (C/D=4, $\gamma D/c_{u0}$=2)

5.3.2 Effects of tunnel burial depth ratio C/D on failure mechanism

Figure 9 indicates that the failure mode of tunnel face under different depths when soil strength heterogeneous and soil weight parameters are fixed ($\rho D/c_{u0}$=1, $\gamma D/c_{u0}$=2). It is clear that as the C/D increases, the width of failure domain at the ground surface increases, the position of collapse near the tunnel face gradually moves down, and collapse domain extends significantly. When C/D increases, the surface overload required to reach the critical instability state also increases. Meanwhile, the surface overload and soil self-weight are the main factors. When the tunnel collapse, the range of failure extends to ground surface, so width of the surface failure domain increases.

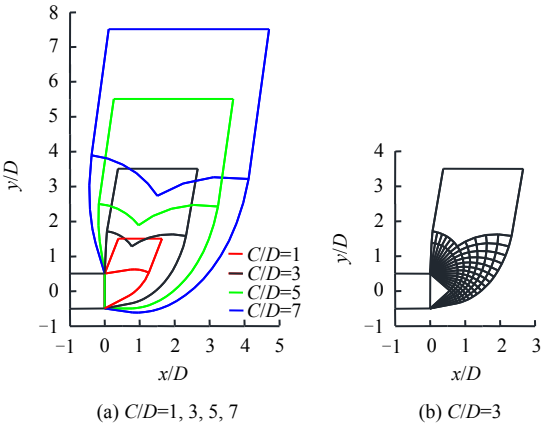

(a) C/D=1, 3, 5, 7 (b) C/D=3

Fig.9 Failure mechanisms of slip line network in tunnel face ($\rho D/c_{u0}$=1, $\gamma D/c_{u0}$=2)

5.3.3 Effect of soil unit weight parameter $\gamma D/c_{u0}$ on failure mechanism

When the tunnel burial depth ratio and soil strength heterogeneous parameters are constant (C/D=3, $\rho D/c_{u0}$= 1), the failure mechanism of tunnel face corresponding to different values of $\gamma D/c_{u0}$ are shown in Fig. 10. The effect of $\gamma D/c_{u0}$ on the failure mode is not obvious, and the outlines of the failure zone remain nearly unchanged.

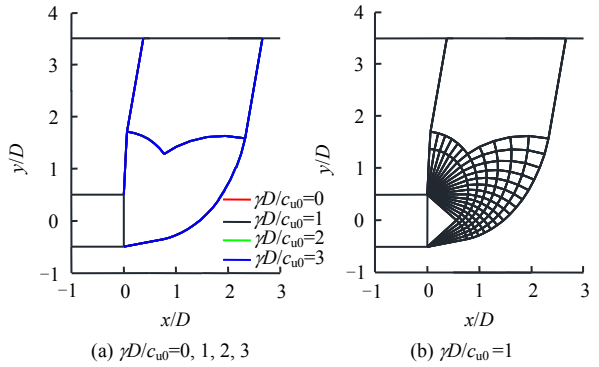

(a) $\gamma D/c_{u0}$=0, 1, 2, 3 (b) $\gamma D/c_{u0}$=1

Fig.10 Failure mechanisms of slip line network in tunnel face (C/D=3, $\rho D/c_{u0}$=1)

6 Conclusions

(1) The critical loads σ_s/c_{u0} increase with an increase in the tunnel depth ratio C/D, and the larger the soil gravity parameters $\gamma D/c_{u0}$ is, the slower the growth rate will be; σ_s/c_{u0} increases linearly with the soil strength heterogeneous parameter $\rho D/c_{u0}$, and the increase rate increases with the increase of the tunnel depth ratio C/D; σ_s/c_{u0} decreases linearly with $\gamma D/c_{u0}$, and the decrease trend increases with the increase of buried depth.

(2) When $\rho D/c_{u0}$ increases, the overall failure zone becomes narrower, the location becomes shallower, and the width of surface failure domain decreases; when C/D increases, the main failure zone increases significantly and extends to the surface; $\gamma D/c_{u0}$ does not show obvious influence on the failure mechanism.

(3) The number and distribution of active discontinuities in the UBFEM-RTME method have an important impact on the accuracy of upper bound solution of critical load σ_s/c_{u0} and associated failure mechanisms. Reasonably selecting the number of active discontinuities and optimizing their distribution form can help effectively improve the accuracy of the upper bound solutions and obtain refined failure mechanisms of tunnel face.

References

[1] DAVIS E H, GUNN M J, MAIR R J, et al. The stability of shallow tunnel and underground openings in cohesive material[J]. Geotechnique, 1980, 30(4): 397−416.

[2] SLOAN S W, ASSADI A. Undrained stability of a square tunnel in a soil whose strength increases linearly with depth[J]. Computers and Geotechnics, 1991, 12(4): 321−346.

[3] WILSON D W, ABBO A J, SLOAN S W, et al. Undrained stability of a circular tunnel where the shear strength increases linearly with depth[J]. Canadian Geotechnical Journal, 2011, 48(9): 1328−1342.

[4] AUGARDE C E, LYAMIN A V, SLOAN S W. Stability of an undrained plane strain heading revisited[J]. Computers and Geotechnics, 2003, 30(5): 419−430.

[5] WILSON D W, ABBO A J, SLOAN S W, et al. Undrained stability of a square tunnel where the shear strength increases linearly with depth[J]. Computers and Geotechnics, 2013, 49: 314−325.

[6] BOONCHAI K, KONGKIT Y, SURAPARB K. Three-dimensional undrained tunnel face stability in clay with a linearly increasing shear strength with depth[J]. Computers and Geotechnics, 2017, 88: 146−151.

[7] ZHOU Wei-xiang, HUANG Mao-song, LÜ Xi-lin. Numerical simulation of minimal support pressure of plane strain tunnel in heterogeneous clays[J]. Rock and Soil Mechanics, 2010, 31(Suppl. 2): 418−421.

[8] LÜ Xi-lin, LI Feng-di, HUANG Mao-song, et al. Three-dimensional numerical and analytical solutions of limit support pressure at shield tunnel face[J]. Journal of Tongji University (Natural Science), 2012, 40(10): 1469−1473.

[9] HUANG Mao-song, SONG Chun-xia. Upper-bound stability analysis of a plane strain heading in heterogeneous clay[J]. Tunnelling and Underground Space Technology, 2013, 38(9): 213−223.

[10] SONG Chun-xia, HUANG Mao-song, LÜ Xi-lin. Upper bound analysis for plane strain tunnel in non-homogeneous clays[J]. Rock and Soil Mechanics, 2011, 32(9): 2645−2650.

[11] HUANG Mao-song, SONG Chun-xia, LÜ Xi-lin. Upper bound analysis for stability of a circular tunnel in heterogeneous clay[J]. Chinese Journal of Geotechnical Engineering, 2013, 35(8): 1504−1512.

[12] YANG F, ZHANG J, YANG J S, et al. Stability analysis of unlined elliptical tunnel using finite element upper-bound method with rigid translatory moving elements[J]. Tunnelling and Underground Space Technology, 2015, 50: 13−22.

[13] YANG Feng, ZHAO Lian-heng, ZHANG Jian, et al. Investigation of finite element upper bound solution based on rigid translatory moving element[J]. Rock and Soil Mechanics, 2014, 35(6): 1782−1786.

[14] SUN Yan-jun, YANG Jun-sheng, LUO Jing-jing, et al. Stability and mesh-like collapse mechanism of tunnel face[J]. Chinese Journal of Geotechnical Engineering, 2019, 41(7): 1374−1380.

[15] SUN Yan-jun, YANG Jun-sheng, YANG Feng, et al. Upper bound finite element analysis of the stability of tunnel faces on the opposite side before penetration[J]. Journal of Harbin Institute of Technology, 2019, 40(7): 1290−1296.

[16] ATKINSON J H, BRANSBY P L. The mechanics of soils: an introduction to critical state soil mechanics[M]. London: McGraw-Hill, 1978.

[17] YANG Feng, ZHANG Jian, ZHAO Lian-heng, et al. Upper-bound finite element analysis of stability of tunnel face subjected to surcharge loading in cohesive-frictional soil[J]. KSCE Journal of Civil Engineering, 2016, 20(6): 2270−2279.